Supplementary Information

Self-sacrificial organic prelithiation additive for high-capacity lithium-ion batteries

Peng Zhao[ab], Shijin Dong[ac], Xuegang Yu[b], Yipin Zhang[ac,]*

[a]Wuxi Zero to Oneto Future New Material Research Institute Co., Ltd, Wuxi, Jiangsu 214181, China

[b]Lab of Functional and Biomedical Nanomaterials, College of Materials Science and Engineering, Qingdao University of Science and Technology, Qingdao 266042, China.

[c]Shenzhen Yanyi New Materials Co., Ltd, Shenzhen, Guangdong, 518000, China.

* Corresponding authors. E-mail addresses: zhangyipin@yanyii.cn (Y. Zhang)

Experimental Section

Synthesis of organic lithium salts

In a typical procedure, Li_2DHPN was synthesized via a rotary evaporation method. First, a mixture of 3,6-dihydroxyphthalonitrile ($C_8H_4N_2O_2$, Adamas) and $LiOH·H_2O$ (Adamas) at a molar ratio of 1:2 was added to deionized water and thoroughly stirred to form a homogeneous aqueous solution. Then, the solvent was separated at 75℃ in a vacuum state by using the rotary evaporation method, grinded the dried sample and the Li_2DHPN powder was obtained. Subsequently, the sample was dried at 150 ℃ to remove the crystallization water and stored under anhydrous condition.

Preparation of MS-LD and Electrodes

The multifunction separator with Li_2DHPN (MS-LD) was prepared by mixing 90 wt.% of Li_2DHPN and 10 wt.% of polyvinylidene difluoride binder (PVDF, Guangdong Hec-al) in N-methyl-2-pyrrolidone (NMP, Adamas). The slurry was uniformly coated onto a PE separator using a mayer rod, followed by vacuum drying at 60 ℃ for 12 h. The coating thickness of the Li_2DHPN was adjusted by varying the solid content of the slurry. The mass loading of Li_2DHPN on the separator was controlled at approximately 0.5 mg cm^{-2}, accounting for 2.6% of the mass of the LFP cathode active material.

The cathodes in half-cell of Li_2DHPN, $LiFePO_4$ (LFP, Longthium Energy) and LFP/Li_2DHPN were prepared by mixing 80 wt.% of active materials, 10 wt.% of Super-P carbon (Sinopharm Chemical Reagent Co), and 10 wt.% of PVDF binder in NMP. The LFP/Li_2DHPN cathode composite was formulated with a mass ratio of 98:2 (LFP: Li_2DHPN) by weight. To prepare the cathodes of full cells, 96.25 wt.% of LFP were mixed with 1.25 wt.% of Super-P carbon and 2.5 wt.% of PVDF binder in NMP. The slurries were uniformly coated onto Al foil, followed by vacuum drying at 90 ℃ for 12 h. The graphite anodes were prepared by mixing 96.2 wt.% of graphite (Jiangxi Zichen Technology Co), 0.6 wt.% of Super-P carbon, 0.6 wt.% of CMC, and 2.6 wt.% of PAA binder in deionized water. The slurry was coated onto Cu foil, and then dried at 90 ℃ for 12 h in a vacuum condition.

Electrochemical Measurements

CR2032 type coin cells were fabricated in an argon-filled glovebox ($O_2/H_2O \leq$ 0.01 ppm) using standardized assembly procedures. The prepared Li_2DHPN, LFP and LFP/ Li_2DHPN as the cathode of the half cells, Li foil (200 μm thickness, 99.9% purity)

served as counter electrodes, with Celgard 2500 polyethylene (PE) membranes employed as separators. The commercial PE separator in the cell was replaced with MS-LD to evaluate the electrochemical performance of the MS-LD, and the Li_2DHPN coating was contacted with the cathode side. Stainless steel gaskets and spring washers were used as the support. The pouch full cells were assembled using double-sided coated graphite anodes (area capacity of 5.59 mAh cm^{-2}) and double-sided coated LFP cathodes (area capacity of 4.9 mAh cm^{-2}) and MS-LD on a semi-automated cell-manufacturing line with a dew point of -45 ℃ and a working temperature of 23 ℃. After activation, the pouch cells were finally sealed after exhausting gas generated during the formation process. For half and full cells，the commercial electrolyte (1 M $LiPF_6$ in a mixture of ethylene carbonate, dimethyl carbonate, and ethyl methyl carbonate with 1:1:1 vol% ratio) was added on each side of separators.

The charge-discharge test of the cells was performed at 25 ℃ using NEWARE and LAND battery test system. CV and EIS measurements of half-cell were conducted on a CHI660e electrochemical workstation. EIS measurements of full cell were conducted on an Arbin tester. For the CV measurement, the scan rate was set at 0.1 mV/s, and for the EIS measurement, the frequency range was from 500 kHz to 0.01 Hz.

Charging and discharging process step of formation: Galvanostatic charge 1 (CI: 60 mA, T: 145 min, UV: 3500mV)→Galvanostatic charge 2 (CI: 360 mA, T: 95 min, UV: 3500mV)→Galvanostatic charge 3 (CI: 396 mA, T: 180 min, UV: 3700mV)→Galvanostatic discharge (CI: 39 mA, T: 300 min, UV: 2000mV)

Material Characterizations

The morphologies of Li_2DHPN and the MS-LD were characterized by field emission scanning electron microscope (SEM, ZEISS Sigma 300), Energy dispersive spectrometer (EDS, Oxford Xplore 30) was used to analyze the elemental distribution of materials. Fourier transform infrared (FTIR) spectra were collected using a Nicolet iS10 in the wavenumber range from 4000 cm^{-1} to 400 cm^{-1}. Nuclear magnetic resonance (NMR) spectra were recorded with a Bruker AVANCE 400 MHz spectrometer. The thermal stability of Li_2DHPN was investigated using a differential scanning calorimeter (DSC, DSC 3500, NETZSCH) and a thermogravimetric analyzer (TGA, TG 209 F3, NETZSCH) in a nitrogen atmosphere, with the temperature raised

from room temperature to 300 ℃ at a rate of 10 ℃ min^{-1}.

Supporting Figures and Tables

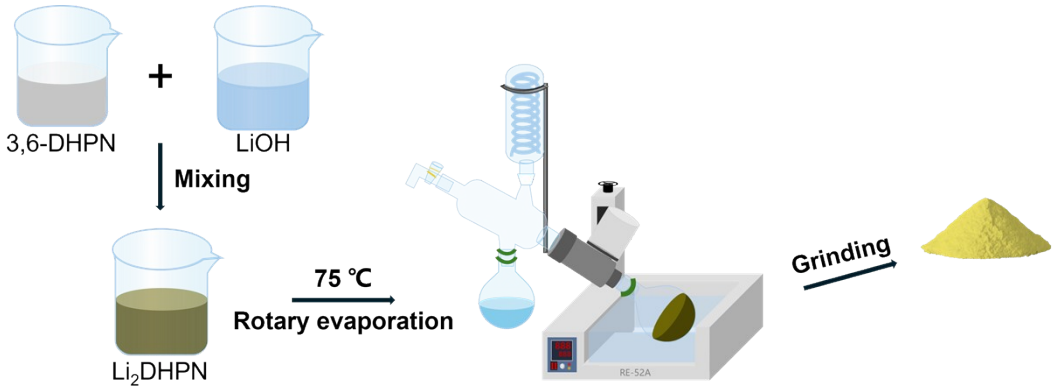

Fig. S1 The synthesis pathway for Li_2DHPN

Fig. S2 Optical image of Li_2DHPN

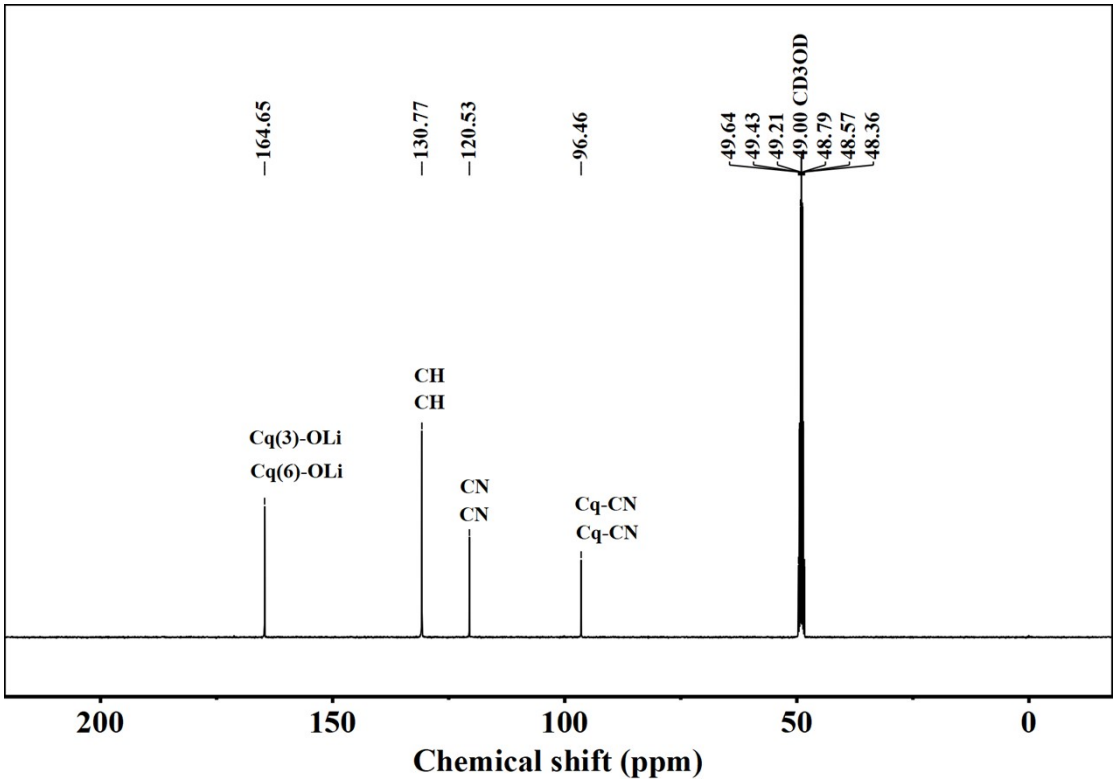

Fig. S3 ^{13}C Nuclear magnetic resonance spectrum of Li_2DHPN at 400 MHz. Methanol-D4 (CD_3OD) was used as the solvent.

The peak at 164.65 ppm can be attributed to the carbon atoms at positions 3rd and 6th connected to -O-Li. The signal at 130.77 ppm represents the two C-H carbon atoms on the benzene ring. The carbon atom on -C≡N can be found at 120.53 ppm, and the peak at 96.46 ppm can be attributed to the two carbon atoms on the benzene ring connected to -C≡N. The peak at 49 ppm is attributed to the methanol solvent (CD_3OD).

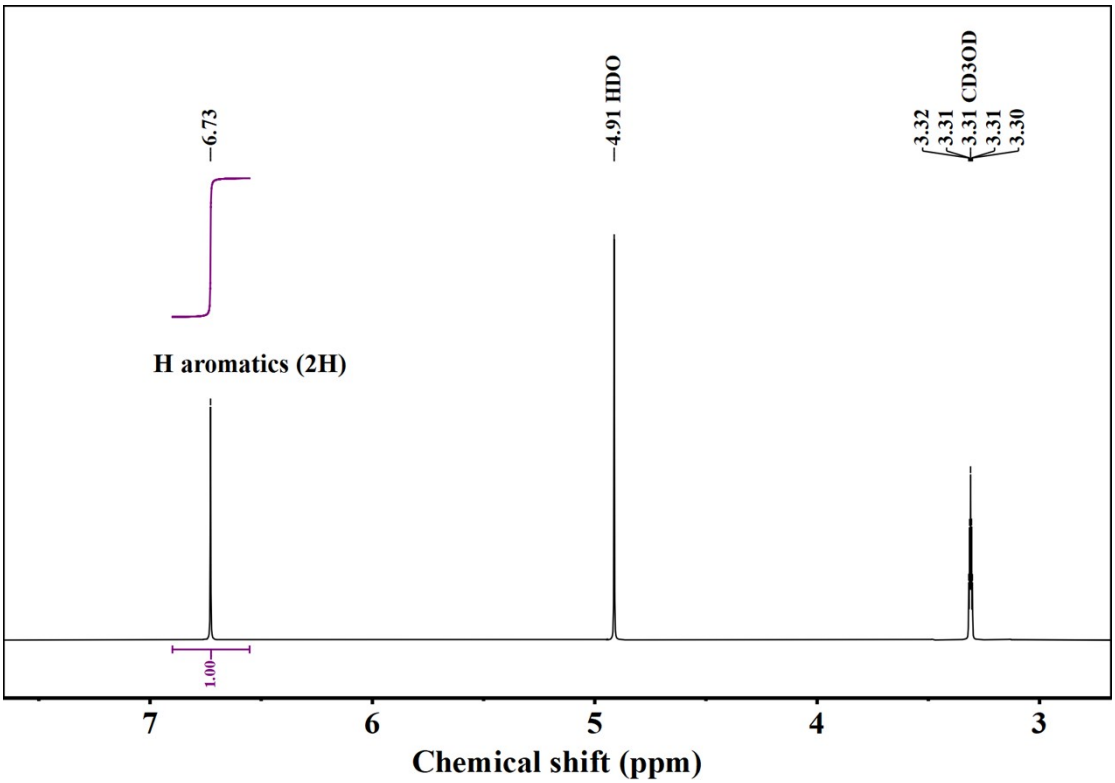

Fig. S4 ^{1}H Nuclear magnetic resonance spectrum of Li_2DHPN at 400 MHz. Methanol-D4 (CD_3OD) was used as the solvent.

The peak at 6.73 ppm can be attributed to the two hydrogen atoms connected to the benzene ring. The peak at 3.31 ppm is attributed to the methanol solvent (CD_3OD). The chemical shift at 4.91 ppm is characteristic of HDO, which might be due to the presence of moisture in the atmosphere or in the deuterated methanol. Additionally, almost no signal of the -O-H hydrogen atom was detected, indicating that the purity of the synthesized Li_2DHPN is very high.

MS (ESI) ($[M^+H]^+$) Calcd. for $Li_2C_8H_2N_2O_2$ 173.05, found 173.0.

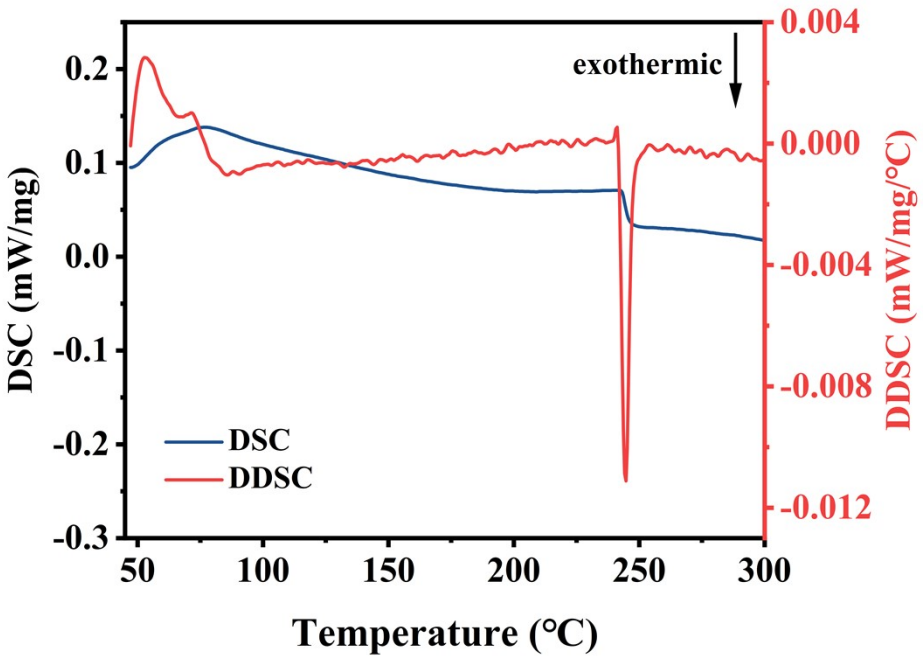

Fig. S5 Differential scanning calorimetry (DSC) thermogram of Li_2DHPN at aheating rate of 10℃ min^{-1}.

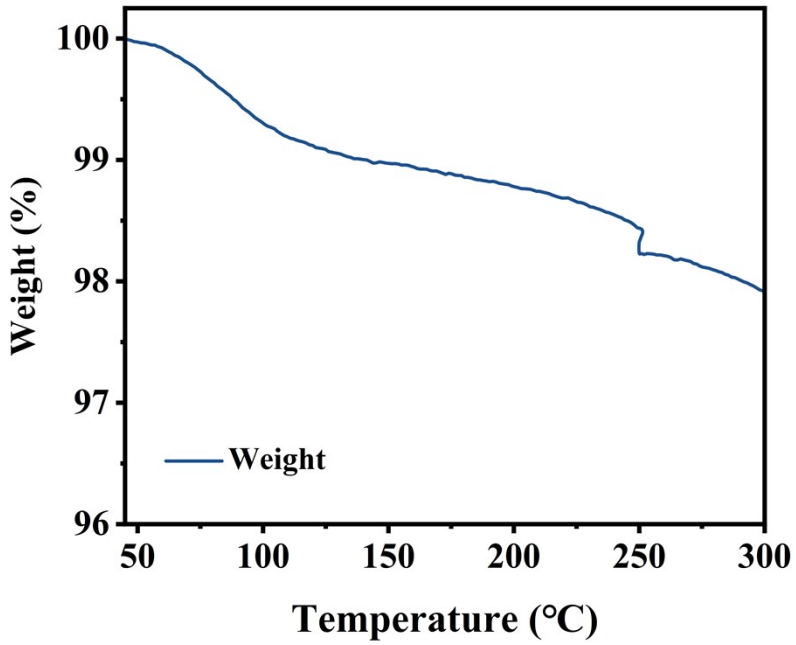

Fig. S6 Thermogravimetry analysis (TG) thermogram of dried Li_2DHPN at a heating rate of 10℃ min^{-1}.

Differential scanning calorimetry (DSC) analysis of the Li_2DHPN sample revealed a prominent exothermic peak at approximately 245 °C (Fig. S5). Concurrently, thermogravimetric analysis (TGA) displayed a distinct weight loss step near this temperature (Fig. S6), suggesting partial thermal decomposition of Li_2DHPN accompanied by gas release. The mass loss observed prior to 245 °C might be attributed to the evaporation of crystallization water formed during the preparation of Li_2DHPN by the rotary evaporation.

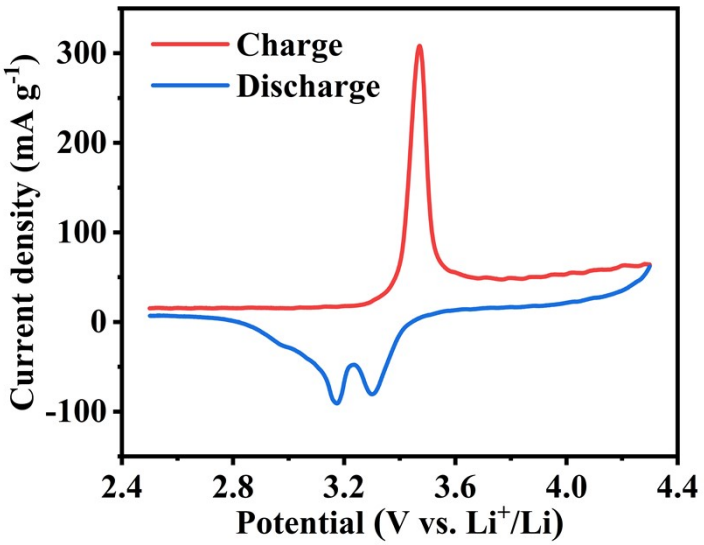

Fig. S7 The CV curves of the initial cycle of Li_2DHPN||Li cell.

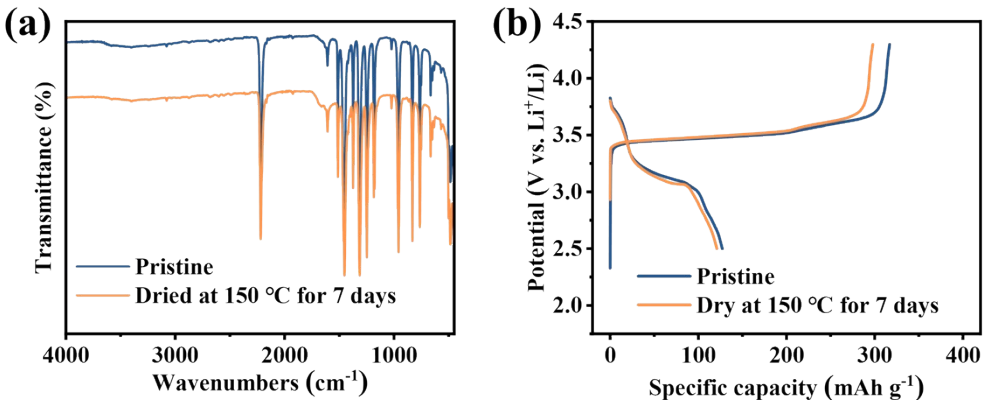

Fig. S8 High-temperature stability of Li_2DHPN in air: (a) FT-IR spectra of Li_2DHPN before and after being dried at 150 ℃ 7 days. (b) Initial charge-discharge profiles of Li_2DHPN||Li cells before and after being dried at 150 ℃ 7 days.

To remove the crystalline water in Li_2DHPN, thermal treatment at 150 °C in air for 7 days was carried out. Structural characterizations and electrochemical performance tests were conducted on the samples before and after drying (Fig. S8). The results showed that there were no obvious changes in the FT-IR spectra of Li_2DHPN and the initial charge-discharge curves of Li_2DHPN||Li half cells before and after the thermal treatment.

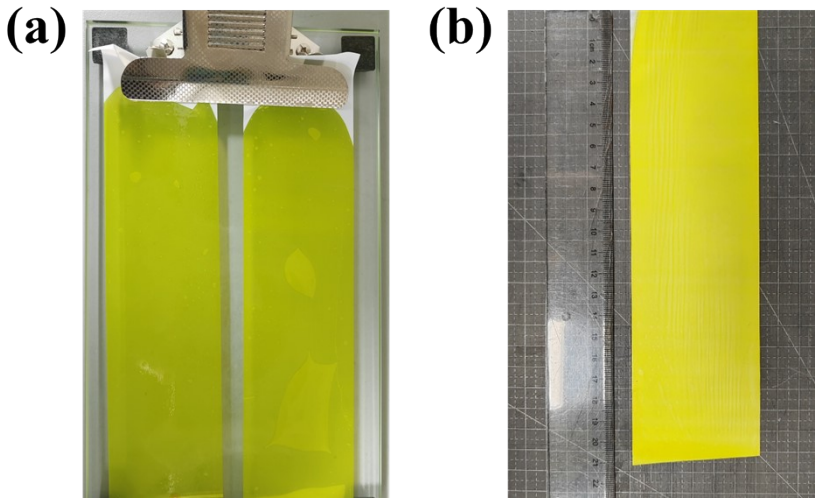

Fig. S9 Optical images of Li_2DHPN coated separator: (a) Before drying; (b) After drying.

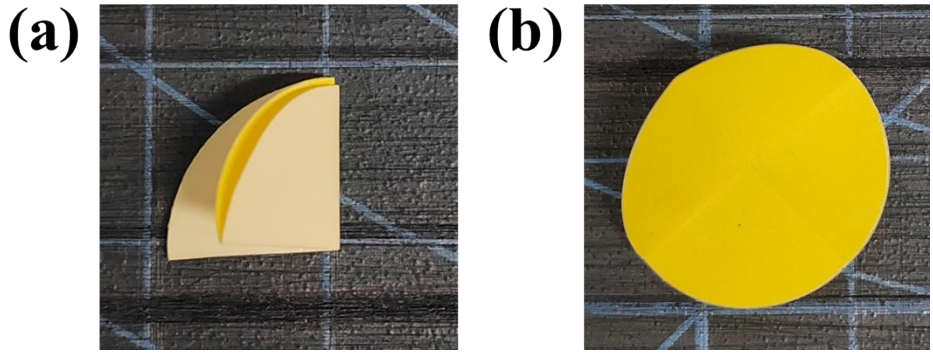

Fig. S10 Optical images of the disc-shaped MS-LD: (a) Folded; (b) Recovery.

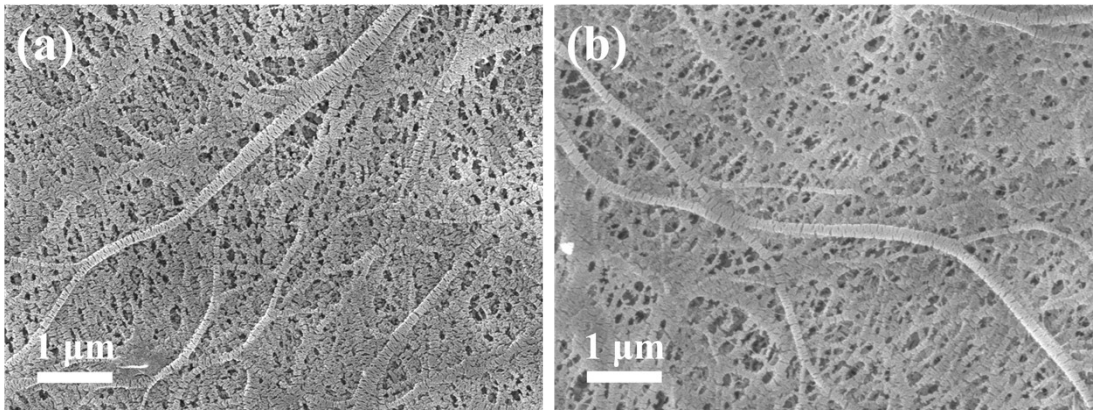

Fig. S11 SEM images of (a) blank side of MS-LD and (b) Commercial PE separator.

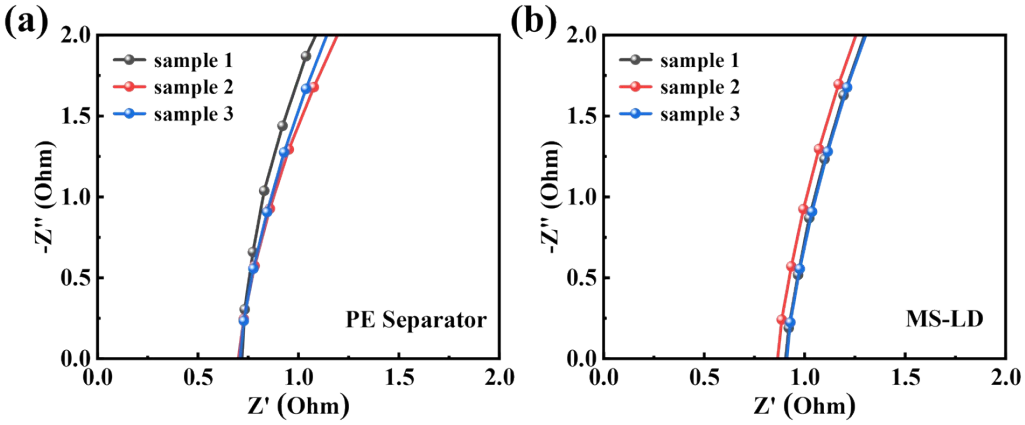

Fig. S12 EIS spectra of (a) PE Separator and (b) MS-LD.

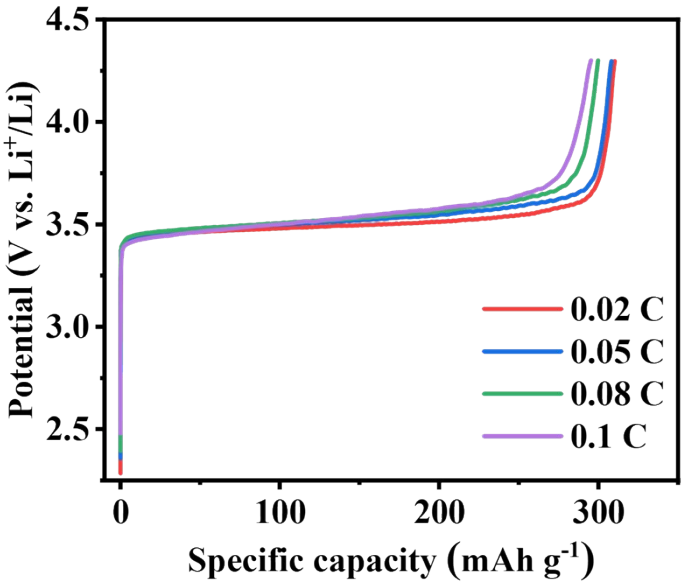

Fig S13 Initial charge profiles of Li_2DHPN||Li half-cell at different C-rate.

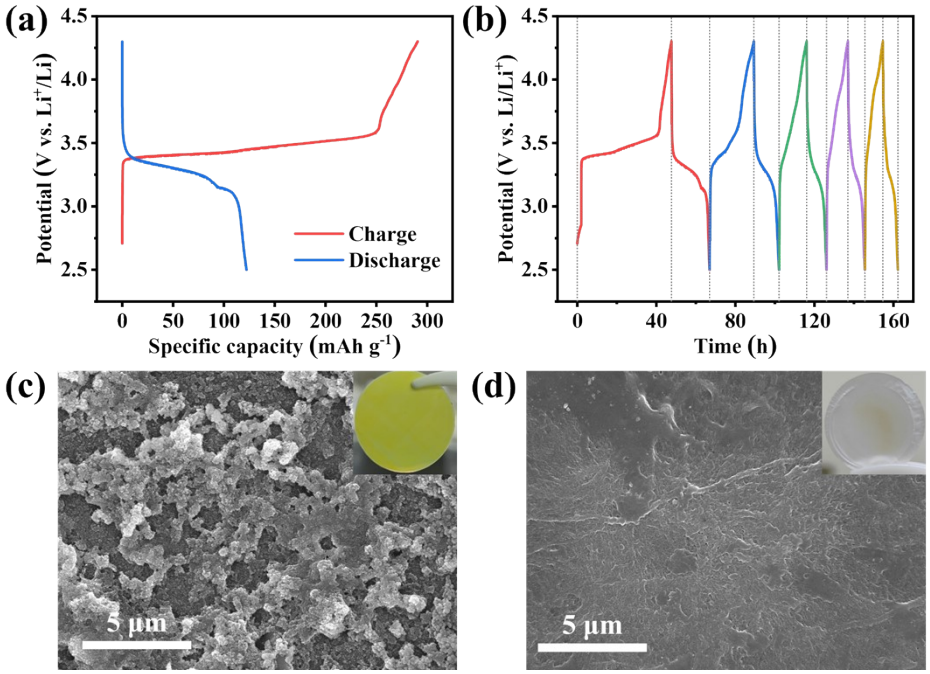

Fig. S14 (a) Galvanostatic charge–discharge profile of Al|MS-LD|Li half-cell in the first cycle. (b) Galvanostatic charge–discharge profiles of Al|MS-LD|Li half-cell in the first five cycles. (c-d) SEM images of the MS-LD before and after cycling.

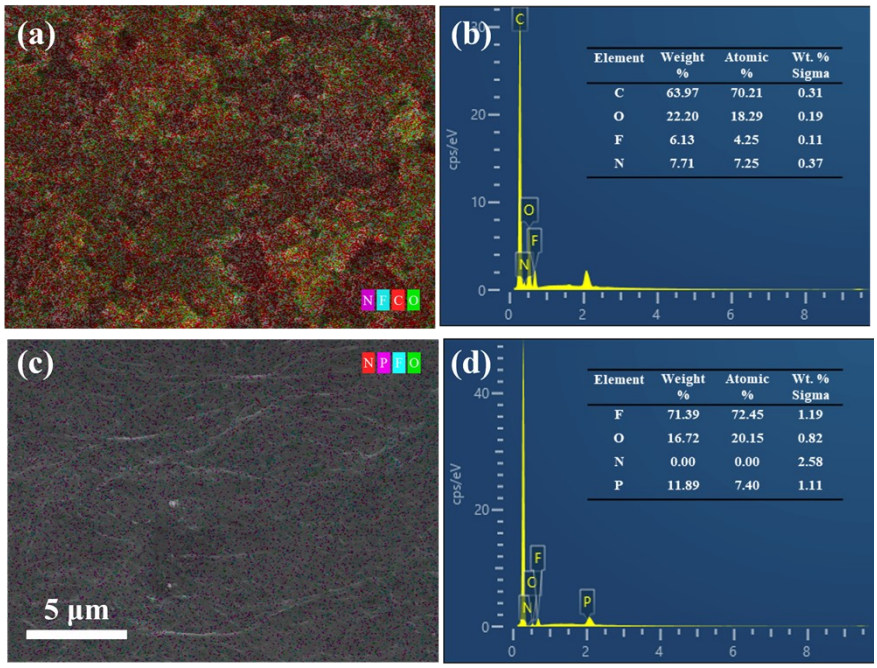

Fig. S15 SEM-EDS images and elemental analysis of the MS-LD: (a)(b) Before cycling (c)(d) After 5th cycle.

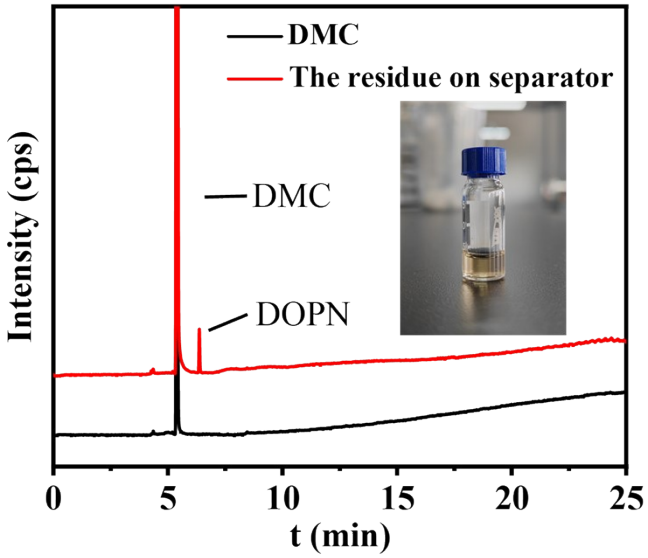

Fig. S16 Gas chromatography (GC) of the residue on separator after cycling dissolved in DMC.

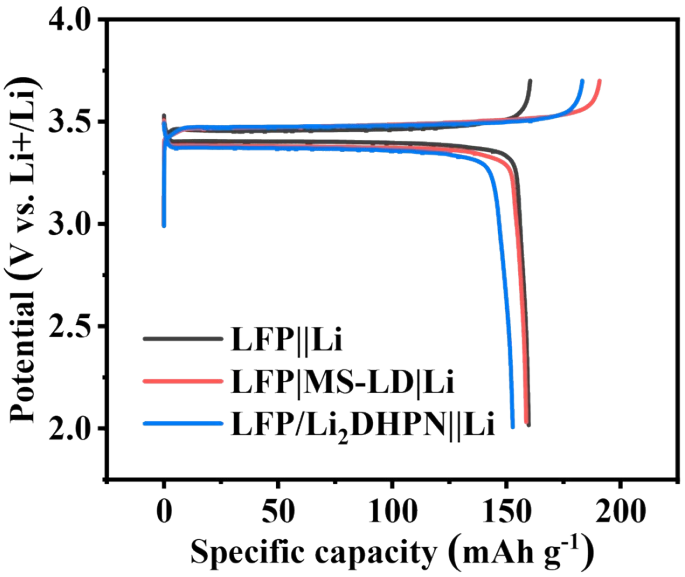

Fig. S17 Initial charge-discharge profiles of LFP||Li, LFP|MS-LD|Li and LFP/Li_2DHPN||Li half cells at 0.1 C.

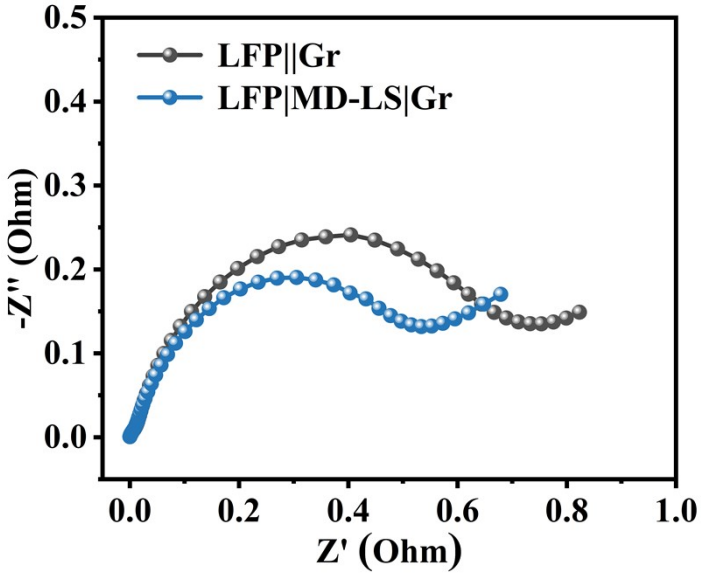

Fig. S18. EIS spectra of LFP||Gr and LFP|MS-LD|Gr full cells at 50% SOC under -10 ℃.

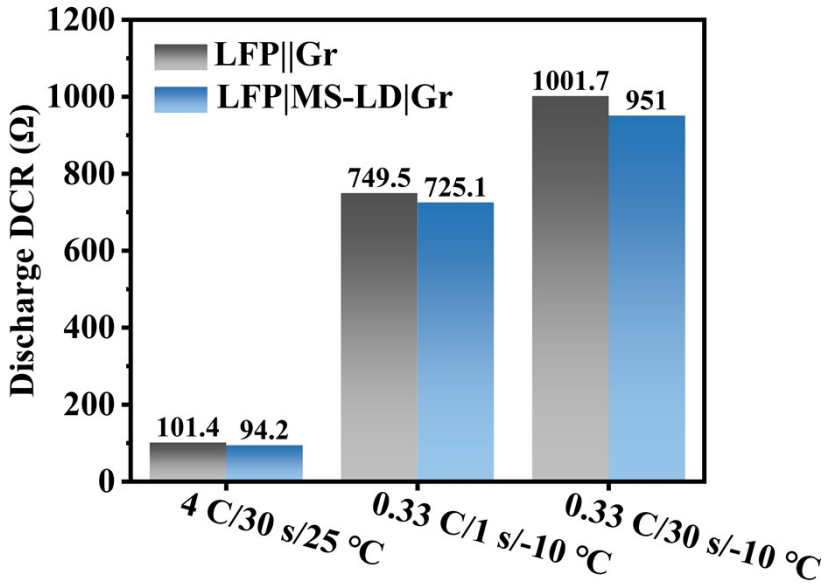

Fig. S19 Comparison of discharge direct current resistance (DCR) of LFP||Gr and LFP|MS-LD|Gr full cells.

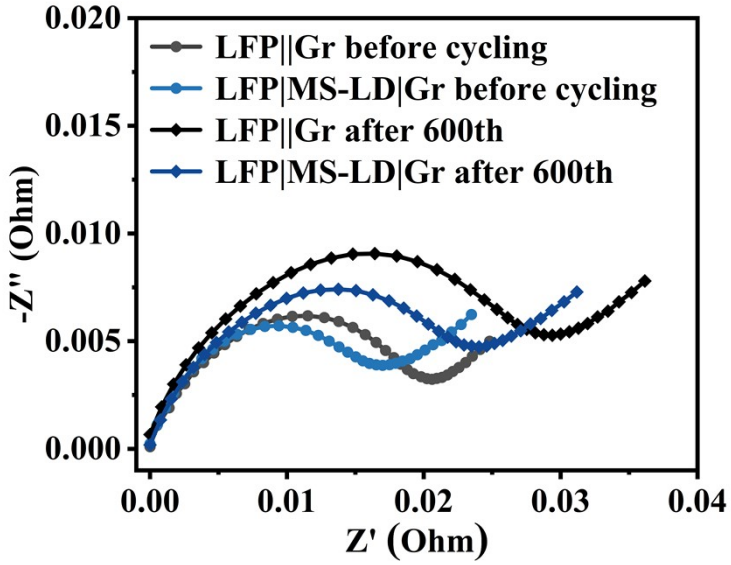

Fig. S20 EIS spectra of LFP||Gr and LFP|MS-LD|Gr full cells before and after cycling.

As shown in Fig. S20, after 600 cycles, the charge transfer resistance (Rct) of both the LFP||Gr and LFP|MS-LD|Gr cells increased compared to their initial states, which is a typical phenomenon associated with long-term cycling-induced interfacial evolution. Notably, the Rct of the LFP|MS-LD|Gr cell remains consistently lower than that of the LFP||Gr cell after extended cycling. This observation provides direct evidence that the beneficial effect of DOPN on interfacial kinetics is not merely transient but is sustained over long-term operation.

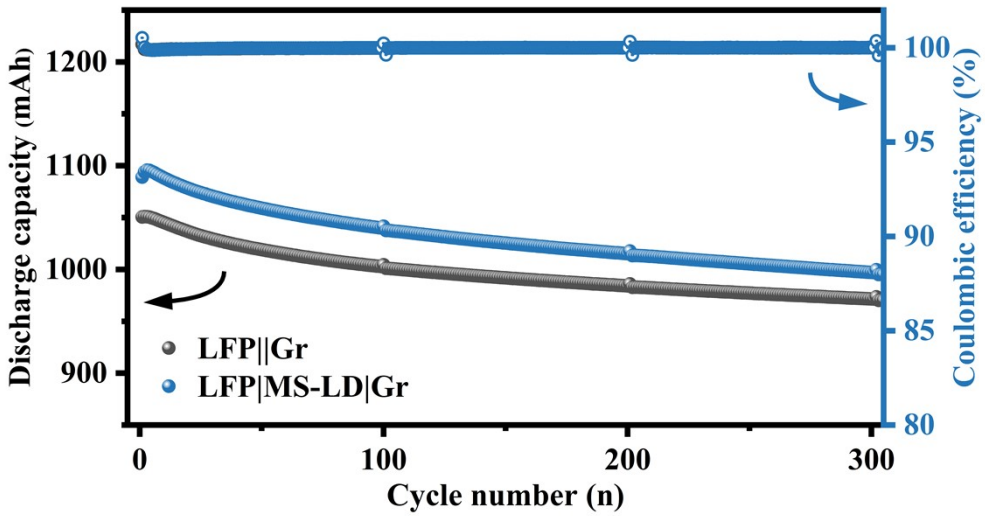

Fig. S21 Cycle stability of LFP||Gr, LFP|FPS|Gr and LFP/Li_2DHPN||Gr full cells at 1 C under 45 ℃.

Separator	Thickness (μm)	Bulk Resistance R_Ω (Ω)	Ionic Conductivity σ ($mS \cdot cm^{-1}$)
PE Separator	18	0.71	0.90
MS-LD	18+5.9 (coating)	0.89	0.95

Tab. S1 Ionic Conductivity of PE Separator and MS-LD.

To characterize the ability of the MS-LD separator to transport lithium ions, we conducted EIS tests on the MS-LD separator and calculated its ionic conductivity. The ionic conductivity of the separators was measured by electrochemical impedance spectroscopy (EIS) using stainless steel (SS) blocking electrodes in a SS|separator|SS symmetric cell. The separators were cut into discs (diameter 19 mm), assembled in a 2032 coin cell in an argon-filled glovebox, and soaked with commercial electrolyte (1 M $LiPF_6$ in EC: DMC: EMC = 1:1:1 by vol.). After 30 min of infiltration to ensure complete wetting, EIS measurements were performed over a frequency range of 1 MHz to 0.1 Hz. The ionic conductivity (σ) was calculated using the equation:

$$\sigma = L/(R_\Omega \times A)$$

where L is the separator thickness (cm), R_Ω is the bulk resistance (Ω) obtained from the high-frequency intercept of the Nyquist plot, and A is the effective area of the stainless steel electrode (cm^2).

As shown in Fig. S12 and Tab.S1, the ionic conductivity of the MS-LD separator is higher than that of the pure PE separator. This enhancement can be primarily attributed to the following factors: First, the Li_2DHPN coating contains strongly polar cyano groups (-C≡N), which exhibit excellent affinity with carbonate-based electrolytes, significantly improving the wettability of the separator surface toward the electrolyte (the contact angle decreases from 29.9° to 18.8°), thereby facilitating Li^+ transport at the separator/electrolyte interface.

Separator	Direction	Tensile Strength (MPa)	Elongation at Break (%)
PE Separator	MD	95.2	45.3
	TD	108.7	38.6
MS-LD	MD	91.6	42.1
	TD	104.3	35.4

Tab. S2 Tensile strength tests of PE Separator and MS-LD.

To further characterize the mechanical strength of MS-LD, tensile strength tests were conducted on MS-LD. The tensile strength of the separators was measured using a universal testing machine following the ASTM D882 standard. The separators were cut into dumbbell-shaped specimens (width 15 mm, gauge length 100 mm) along both the machine direction (MD) and transverse direction (TD). During the test, samples were clamped with rubber-faced pneumatic grips to prevent slippage and damage. Then stretched at a constant speed of 50 mm min^{-1} until breakage. The tensile strength (MPa) and elongation at break (%) were recorded and averaged from at least five parallel specimens.

The results demonstrate that the mechanical strength of the MS-LD separator decreases by approximately 3–5% compared to the pristine PE separator, with no significant deterioration in tensile properties along either the machine direction (MD) or transverse direction (TD). The Li_2DHPN coating adheres firmly to the PE substrate (as shown in Fig. S10) without compromising the overall mechanical integrity of the separator. This conclusion is further supported by the excellent long-term cycling stability of the LFP|MS-LD|Gr full cell (~90.6% capacity retention after 600 cycles, Fig. 4e), which indirectly confirms that the separator maintains its structural integrity during prolonged operation without rupture or internal short circuits.

Tab. S3 Discharge Direct Current Resistance (DCR) of LFP||Gr and LFP|MS-LD |Gr cells at 50%

Sample	No.	DCR at 50%SOC		
		4C/30s/25℃	0.33C/1s/-10℃	0.33C/30s/-10℃
LFP||Gr	1	102.35	758.02	1011.65
	2	101.13	745.68	999.69
	3	100.72	744.65	993.88
	Avg.	**101.40**	**749.45**	**1001.74**
LFP|FPS|Gr	1	91.58	706.93	930.63
	2	94.78	738.82	968.3
	3	96.13	729.39	954.01
	Avg.	**94.16**	**725.05**	**950.98**

SOC.

Tab. S4 Discharge capacity and specific capacity of LFP||Gr and LFP|MS-LD|Gr cells in different

C-rate	LFP|MS-LD|Gr		LFP||Gr	
	Capacity (mAh)	Specific Capacity (mAh g^{-1})	Capacity (mAh)	Specific Capacity (mAh g^{-1})
0.33 C	1104.1	153.3	1079.2	149.9
1 C	1083.9	150.5	1044.9	145.1
2 C	1052.5	146.2	1007.5	139.9
3 C	1032.3	143.4	988.5	137.3
0.33 C (return)	1092.1	151.7	1069.9	148.6

C-rate.